Asian Journal of Chemistry; Vol. 38, No. 5 (2026), 1117-1126
ASIAN JOURNAL OF CHEMISTRY
https://doi.org/10.14233/ajchem.2026.35474

Interfacial Modulation and Capacity Improvement of Ni-Cd Cells using an Oxadiazole based Electrolyte Additive

P. PALANI MURUGAN[1], P. SAKTHIVEL[2], T. SURESH[3], K. VELUMANI[1], C. NIRMALA[4], M. OBULICHETTY[5], S.S. SUBRAMANIAN[5], S. ANNAPOORANI[6], S. MANIKANDAKUMAR[1], A. SELVARAJ[7] and S. RAMESHKUMAR[1,*]

[1]Department of Chemistry, Sri Vasavi College, Erode-638316, India
[2]Department of Nano Science and Technology, Bharathiar University, Coimbatore-641046, India
[3]Department of Chemistry, Bharathiar University, Coimbatore-641046, India
[4]Department of Chemistry, Akshaya College of Engineering and Technology, Kinathukadavu-642109, India
[5]Department of Applied Science, PSG College of Technology, Coimbatore-641004, India
[6]Department of Chemistry, LRG Government Arts College for Women, Tiruppur-641604, India
[7]Department of Chemistry, CBM College, Coimbatore-641042, India

*Corresponding author: E-mail: srksvc2016@gmail.com

Received: 16 December 2025 *Accepted*: 26 February 2026 *Published online*: 4 May 2026 AJC-22335

This work investigates the influence of the heterocyclic organic additive 5-(4-dimethylamino)phenyl-1,3,4-oxadiazole-2(3*H*)-thione on the electrochemical behaviour of Ni-Cd cells in 35% KOH electrolyte. The compound was synthesised in a two-step process using 4-(*N*,*N*′-dimethylamino)methyl benzoate and hydrazine hydrate. Its structure was confirmed by Fourier-transform infrared (FTIR) and nuclear magnetic resonance (NMR) spectroscopy. The electrochemical impedance spectroscopy, cyclic voltammetry and chronoamperometry demonstrated a distinct decrease in charge-transfer resistance, increase in the ion diffusion and higher reversibility of both the $Ni(OH)_2$/NiOOH and $Cd/Cd(OH)_2$ redox couples in the presence of the additive. Successive cycle charge-discharge studies show that in the later cycles there is a higher discharge potential, increased stability and better capacity retention of the cells compared to blank and CMC-modified cells. Capacity output tests also indicate that the additive inhibits the formation of $Cd(OH)_2$ and $Cd(OH)_2$ in the porous electrode matrix, polarisation and effective exploitation of the active material, especially at low and moderate discharge rates. Based on the results, it is confirmed that 5-(4-dimethylamino)phenyl-1,3,4-oxadiazole-2(3*H*)-thione functions as an effective electrolyte modifier, significantly enhancing electrode kinetics, cycling stability and discharge performance in Ni-Cd systems, thereby provides a viable pathway to enhance the performance of alkaline batteries.

Keywords: Ni-Cd battery, Electrolyte additive, 1,3,4-Oxadiazole-2-thione, Charge discharge properties.

INTRODUCTION

Nickel-cadmium (Ni-Cd) battery systems have continued to dominate other mobile devices, emergency lighting systems and aerospace use in their products as nickel-cadmium cation-anode systems have strong cycling characteristics, can handle overcharge and their performance is less affected by the wide temperature range [1,2]. Electrochemical properties of these systems, however, highly rely on the composition and stability of the alkaline electrolyte used to conduct operation [3]. The electrolyte is commonly KOH, although its characteristics can be enhanced substantially by selective incorporation of organic or heterocyclic components that have an effect on electrode kinetics and discharge-charge behaviour [4,5].

Electron-rich functional groups in organic heterocyclic compounds have become the focus of growing interest to electrolyte modification since they are capable of increasing ionic conductivity, suppressing the parasitic reactions and stabilizing electrode-electrolyte interfaces [6]. Most of them are derivatives of 1,3,4-oxadiazole, which have displayed promising electrochemical behaviour due to their excellent capability of donating electrons, planar conjugated structures and capability of engaging in proton-transfer equilibria [7,8]. These molecules can play the role of mediators, corrosion inhibitors or charge-transfer facilitators in the alkaline environment [9].

Compound 5-(4-(dimethylamino)phenyl)-1,3,4-oxadiazole-2(3*H*)-thione is of considerable interest due to its thione-

This is an open access journal, and articles are distributed under the terms of the Attribution 4.0 International (CC BY 4.0) License. This license lets others distribute, remix, tweak, and build upon your work, even commercially, as long as they credit the author for the original creation. You must give appropriate credit, provide a link to the license, and indicate if changes were made.

thiol tautomerism, high electron density and resonance-stabilised aromatic structure [10], which may play a significant role in modulating electrode kinetics in the Ni-Cd systems. The introduction of electron-rich heterocyclic additives containing active functional groups into alkaline electrolytes can alter the characteristics of the electrical double layer, potentially suppressing oxygen evolution at the positive electrode while enhancing faradaic charge-transfer reactions during cycling [11,12]. Moreover, its molecular configuration supports strong adsorption onto electrode surfaces, which may reduce self-discharge and enhance discharge capacity, even at the ambient temperature [13].

While heterocyclic additives have demonstrated notable advantages, there is a lack of detailed and systematic research on the impact of oxadiazole-based thione derivatives on the electrochemical behaviour of Ni-Cd systems [14]. In this context, the inclusion of 5-(4-dimethylaminophenyl)-1,3,4-oxadiazole-2(3*H*)-thione in alkaline electrolytes can offer meaningful insights into improving conductivity, electrode stability, energy efficiency and the cycling behaviour of Ni-Cd cells at ambient conditions. This research is designed to determine its contribution to change the electrolyte behaviour and increasing the performance measures of the Ni-Cd system at room temperature.

EXPERIMENTAL

All chemicals employed in this study were of analytical reagent (AR) grade and used without further purification unless specified. 4-(*N*,*N*-Dimethylamino)methyl benzoate (≥99%) and hydrazine hydrate (80%) were procured from Sigma-Aldrich. Carbon disulfide (≥99.5%) and potassium hydroxide pellets (≥85%) were obtained from Merck. Ethanol (≥99.9%, HPLC grade) and glacial acetic acid (≥99.7%) were supplied by Thermo-Fisher Scientific. Sodium hydroxide (≥98%) used for electrode treatment was purchased from Loba Chemie. All aqueous solutions were prepared using deionised water with a resistivity of 18.2 MΩ cm.

Characterization: FTIR (Perkin-Elmer Spectrum Two, 4000-400 cm^{-1}) and NMR (Bruker Avance III 400 MHz) were used for the structural characterisation. Electrochemical studies (CV, EIS, CA) were carried out on a Zahner Zennium XC workstation using a three-electrode system with Ni-Cd working, platinum counter and Hg/HgO reference electrodes in alkaline medium. The charge-discharge cycling were performed at 27 ± 5 ºC, with voltage recorded at regular intervals.

Synthesis of 5-(4-(dimethylamino)phenyl)-1,3,4-oxadiazole-2(3*H*)-thione: 5-(4-(Dimethylamino)phenyl)-1,3,4-oxadiazole-2(3*H*)-thione was synthesised *via* a two-step procedure. In the first step, hydrazine hydrate was reacted with 4-(*N*,*N*′-dimethylamino)methyl benzoate in a 1:1 molar ratio in alcohol (5 mL) as solvent. The reaction mixture was refluxed for 2 h to facilitate the formation of the corresponding hydrazide intermediate. Upon completion, the mixture was cooled and the resulting solid was separated by filtration, thoroughly washed and dried. In the second step, this intermediate was dissolved in ethanol, followed by the addition of an aqueous KOH solution and CS_2. The reaction mixture was heated and maintained under reflux for an additional 2 h to promote cyclisation. After cooling, the mixture was poured into cold water and subsequently acidified with glacial acetic acid to obtain desired product as precipitate (**Scheme-I**). The obtained solid was filtered, recrystallised from ethanol and washed with water to yield the purified compound.

Preparation of electrolyte: 4-(Dimethylamino)benzohydrazide and 5-(4-(dimethylamino)phenyl)-1,3,4-oxadiazole-2-(3*H*)-thione (2.7009 g) was dissolved in 400 mL of 35% KOH solution with gentle heating to ensure complete dissolution. The resulting solution was filtered to remove any undissolved impurities and the clear filtrate was collected.

Formation of electrodes: Electrochemically impregnated electrodes were prepared by initially treating them in 20% NaOH solution to remove surface impurities including carbonates. The plates were subsequently rinsed in hot water and then immersed in a hot nitrate solution, followed by thorough washing for 4-5 h to eliminate residual ions. Finally, the absence of nitrate impurities was verified using the brucine test with dilute sulphuric acid, indicated by no development of pink colouration.

Filling of electrolytes: The electrodes were assembled following standard procedures and the prepared electrolyte (35% KOH) was gradually introduced into the Ni-Cd cells up to the required level. Two cells were filled for the comparison of experimental results. The number of the cells with and without additives were prepared for comparative evaluation.

Formation cycles: Following electrode assembly, the cells were subjected to three formation cycles conducted at an ambient temperature of 27 ± 5 ºC. Prior to charging, the electrolyte level was adjusted to coincide with the top surface of the electrodes, and the cells were fitted with valve bodies to ensure the controlled operations. Charging was carried out under constant current conditions, with voltage recorded at

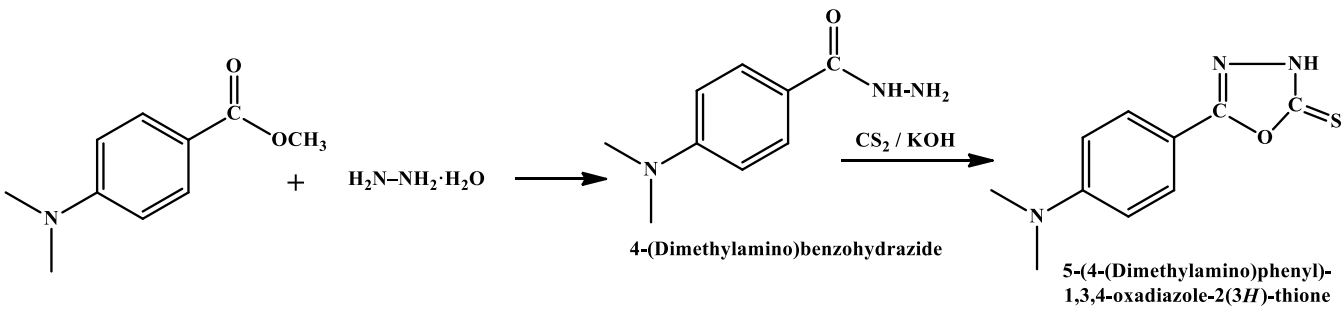

Scheme-I: Synthesis of 4-(dimethylamino)benzohydrazide and 5-(4-(dimethylamino)phenyl)-1,3,4-oxadiazole-2(3*H*)-thione

regular intervals. At the end of each charging step, the electrolyte level was readjusted up to the cover trap, followed by a resting period of 2-4 h. After each discharge, drain clips were introduced to maintain proper cell functioning.

The electrochemical performance was subsequently evaluated through five test cycles (TCs). Each cycle involved charging at 10 A for 5 h followed by 5 A for 3 h, resulting in a total charging duration of 8 h per cycle. After charging, the cells were allowed to rest for a minimum of 12 h before being discharged at a constant current of 25 A down to a cut-off voltage of 1 V. Charging and discharging voltages were monitored at regular time intervals using a Zahner Zennium XC electrochemical workstation. Comparative analysis of cell performance was conducted across successive test cycles to assess the effect of the electrolyte additive. The formation cycles involve stepwise charging at controlled current levels (5-10 A) followed by discharge up to a cut-off voltage of 1 V, enabling gradual activation of the electrodes. An increase in the current during successive cycles improves electrode conditioning, ensuring stable electrochemical performance and efficient capacity development and the details are shown in Table-1.

TABLE-1
FORMATION CYCLES AT DIFFERENT CURRENTS

		Current	Duration
FC_1	Charging	5 A	8 h
	Discharging	5 A	Up to 1 V
FC_2	Charging	10 A	3 h
		5 A	2 h
	Discharging	5 A	Up to 1 V
FC_3	Charging	10 A	3 h
		5 A	2 h
	Discharging	25 A	Up to 1 V

Electrode characteristics: The electrode behaviour was characterised using electrochemical impedance spectroscopy (EIS), cyclic voltammetry (CV) and chronoamperometry (CA), followed by charge-discharge cycling in cells with and without the electrolyte additive. During cycling, the potentials of both positive and negative electrodes were recorded at regular intervals against a standard mercury reference electrode after the initial cycle. The data were represented as voltage-time profiles, with time on the *x*-axis and voltage on the *y*-axis. Based on these measurements, a comparative evaluation was performed between additive-containing and control cells, and variations in performance across successive test cycles were analysed.

RESULTS AND DISCUSSION

The structure of 5-(4-(dimethylamino)phenyl)-1,3,4-oxadiazole-2(3*H*)-thione was characterized by FTIR and NMR spectra presented in Fig. 1. It is evident in the FTIR spectrum of the compound that the N-H stretching of the heterocyclic thioamides/amide-type NH are often to be found as the broad band in the 3500-3200 cm^{-1} region [15,16]. The strong band in the 1000-100 cm^{-1} known as aromatic C–H phenyl ring and oxadiazole ring proton is observed as a weak band in the range 3100-3000 cm^{-1} [16]. The aliphatic C–H stretching of $N(CH_3)_2$ group bonded appears in the form of weak shoulders in the 2950-2850 cm^{-1} [2]. The 1,3,4-oxadiazole ring exhibits a strong characteristic absorption at 1668 cm^{-1}, attributed to C=N/C=C stretching vibrations. In addition, the ν(C=N) and aromatic C=C stretching bands typically appear within the range of 1680-1520 cm^{-1} in 1,3,4-oxadiazole derivatives [17]. The presence of the additional aromatic C=C stretching bands of the *para*-substituted phenyl ring is verified by the presence of peaks at 1584 and 1445 cm^{-1} as the additional aromatic C=C stretching bands. An intermediate peak of 1356 cm^{-1} is related to C–N stretch/CH_3 deformation of the dimethylamino group [16]. In tertiary aromatic amines, ν(C–N) and CH_3 bending is exhibited in the 1360-1250 cm^{-1} region. The overlapping bands of C=S of the thione group and C–O–C/C–N vibrations of the oxadiazole ring give the peaks at 1292 cm^{-1} and 1224 cm^{-1}, respectively [18,19]. In oxadiazole-containing compound, the C–O–C linkage typically exhibits absorption bands in the regions 1275-1200 cm^{-1} and 1075-1020 cm^{-1}, while the

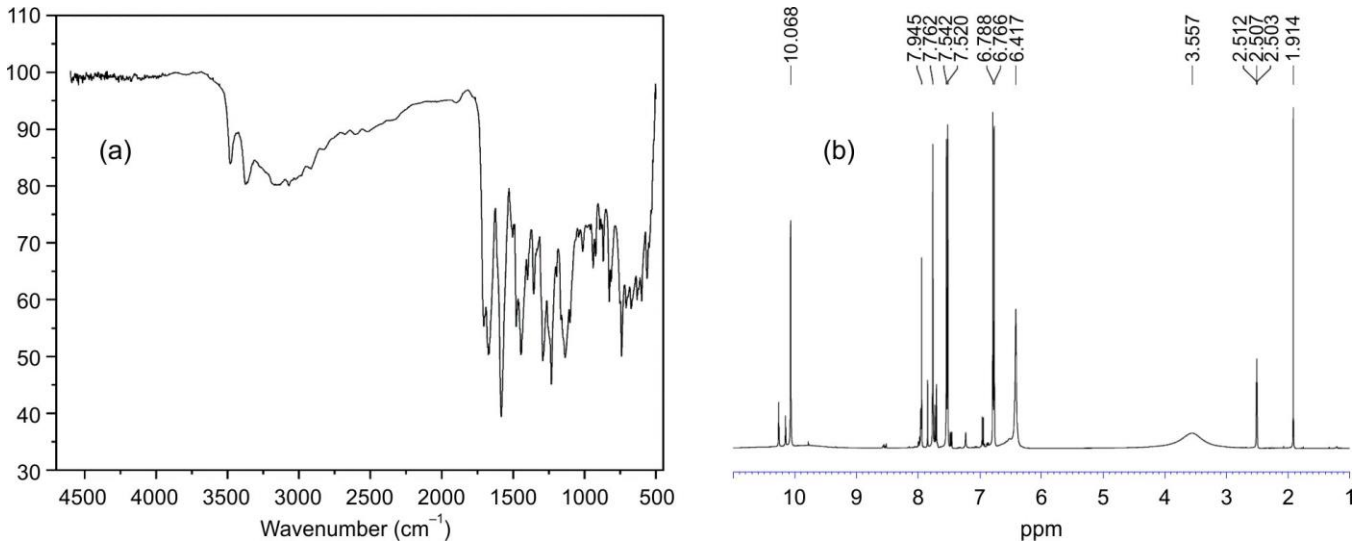

Fig. 1. FT-IR and NMR spectra of synthesised 5-(4-(dimethylamino)phenyl)-1,3,4-oxadiazole-2(3*H*)-thione

ν(C=S) stretching vibration is generally observed around 1270-1220 cm^{-1} [18,19]. The combined C–N and C–O stretching vibrations associated with the dimethylamino group and the oxadiazole ring appear near 1136 cm^{-1} [18,19]. The out-of-plane C–H bending vibrations of the *para*-disubstituted benzene ring and the heteroaromatic system are appeared at 993, 890, 827 and 741 cm^{-1}. Aromatic C–H out-of-plane deformations typically occur within the 900-650 cm^{-1} range, displaying the characteristic multiple bands indicative of *para*-substitution.

In the ^{1}H NMR spectrum, the N–H proton of the 1,3,4-oxadiazole-2(3*H*)-thione tautomer appears as a singlet at δ 10.07 ppm. This resonance is consistent with the characteristic downfield shift (δ 10-13 ppm) observed for such systems, arising from strong deshielding effects induced by the adjacent C=S group and ring nitrogen atoms. The aromatic region exhibits signals corresponding to the *para*-disubstituted phenyl ring. The protons at positions H-2 and H-6, located *ortho* to the electron-withdrawing oxadiazole-2-thione moiety, appear as a pair of doublets in δ 7.95-7.75 ppm region, which is typical for *ortho*-aromatic protons in such environments. The remaining aromatic protons (H-3 and H-5) of the *para*-dimethylaminophenyl group give rise to two doublets at δ 7.54-7.52 ppm and δ 6.79-6.42 ppm. The observed splitting pattern reflects the *para*-substitution, with one set appearing relatively deshielded and the other more shielded due to the strong electron-donating nature of the dimethylamino group. Furthermore, the two equivalent methyl groups of the dimethylamino substituent [$N(CH_3)_2$] were observed as a singlet at δ 3.56 ppm. Typically, N-CH_3 protons resonate in the range δ 2.9-3.1 ppm in less polar solvents; however, a downfield shift to approximately δ 3.5 ppm in DMSO-d_6 is expected due to increased deshielding in the highly polar solvent environment.

EIS, chronoamperometry and CV behaviour of Ni-Cd cell with and without additive: Electrochemical impedance spectroscopy (EIS), cyclic voltammetry (CV) and chronoamperometry present some complementary information on the impact of the additive on the electrochemical behaviour of the Ni-Cd cell. In the Nyquist plots (Fig. 2), the two systems have a depressed semicircle followed by the short low-frequency tail that is usually associated with a Randles-type of equivalent circuit that includes solution resistance, charge-transfer resistance (R_{ct}) and diffusion elements (Fig. 3) [20-22]. The cell without additive shows a significantly larger semicircle, revealing a higher R_{ct} and stronger interfacial polarisation at the electrode–electrolyte interface, represented by constant phase element (CPE) [23,24]. In contrast, the additive containing electrolyte displays a much smaller semicircle, indicating a substantial reduction in R_{ct} and faster charge-transfer kinetics associated with the $Ni(OH)_2$/NiOOH and $Cd/Cd(OH)_2$ redox couples [21,24,25]. Since, the high frequency intercept changes only slightly, the additive mainly influences interfacial rather than bulk ohmic resistance [26].

To balance interfacial modification factors with the idea of transporting electrolytes, the oxadiazole-based additive concentration was kept at 0.5 (w/v). In this concentration, the electrode has gotten coverage on its surface large enough to enable charge-transfer kinetics and inhibit parasitism reactions,

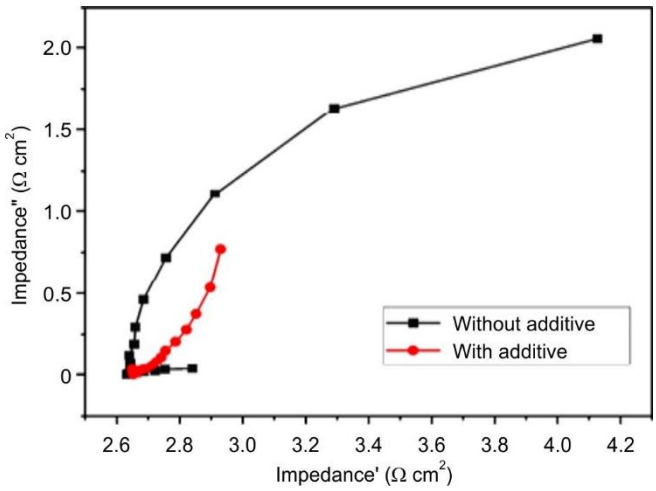

Fig. 2. Nyquist plots for the Ni–Cd cell in the absence and presence of oxadiazole additive

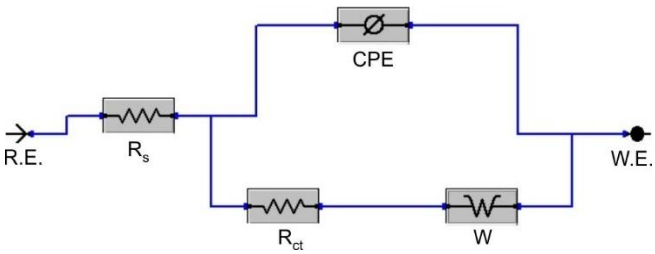

Fig. 3. An equivalent circuit for nyquist plots recorded for Ni–Cd cell in the absence and presence of oxadiazole additive

as is indicated by the dramatic decrease in charge-transfer resistance, an increase in redox reversibility and an increase in discharge properties. The weaker interfacial effect would be expected with lower concentrations, which would offer incomplete surface coverage, whereas higher concentrations might raise electrolyte viscosity, excessive surface adsorption or mass-transport constraints, which have the potential to bring a negative effect of electrode accessibility. Widely reported similar optimum concentration windows of the heterocyclic electrolyte additives have applied to alkaline battery systems, where moderate levels of additives satirize the highest kinetic advantage but do not bring about surface blocking. Thus, 0.5% is a viable and practically useful concentration that provides an actual enhancement of performance without negative effects on electrolyte conductivity and stability.

The lower tail observed at the low-frequency when the additive is present indicates enhanced diffusion of ion and enhanced infiltration of the electrolyte in the porous active material [24,27]. Generally, the Nyquist plots justify that the additive intensifies electrode kinetics, interfacial resistance and electrochemical accessibility of active species that are essential in Ni-Cd systems at high-rate operation [25].

The additional proof on the beneficial effect of the additive is the result of the chronoamperometric curves (Fig. 4). The observed current decay following the potential step is of the usual diffusion-controlled Cottrell behaviour [28,29]. Nevertheless, the additive cell has a permanently negative current within the period of transience. The lower cathodic transient current is described by the inhibition of parasitic side reactions, especially the hydrogen evolution process and the

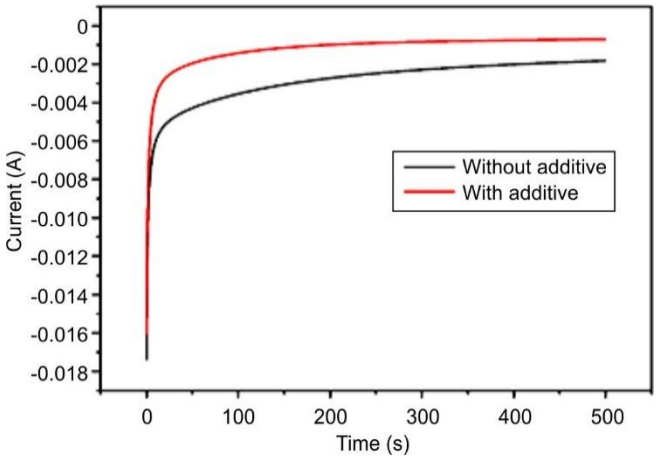

Fig. 4. Chronoamperometric curves for the Ni–Cd cell in the absence and presence of oxadiazole additive

metal dissolution process that frequently primarily happens in alkaline systems with nickel within the primary charge-discharge reaction; the results of the EIS and CA clearly demonstrate the presence of better kinetics of primary charge-discharge reaction [30,31]. Therefore, the additive acts as a protective interfacial modifier, which reduces self-discharge and improves coulombic efficiency.

These conclusions are further supported by the cyclic voltammograms (Fig. 5). The observed peaks are attributed to the $Cd/Cd(OH)_2$ and $Ni(OH)_2/NiOOH$ redox transitions, and are evident in both electrolytes [32-34]. The peak currents are lower without additive and so is the peak separation, which represents slow kinetics or high polarisation. Upon the introduction of the additive, the anodic and cathodic peak current and separation of two peaks are observed to increase and the reduction in charge-transfer between the peaks, respectively and the reversibility is enhanced and the processes are observed to be faster [32,35]. The increased area under the CV curve in the additive-containing system reflects improved active material utilisation and higher charge storage capability [33, 35]. Such improvements are consistent with the previous reports showing that electrolyte additives stabilize electrode surfaces, promote the formation of highly conductive phases and enhance overall battery performance [26,35-37].

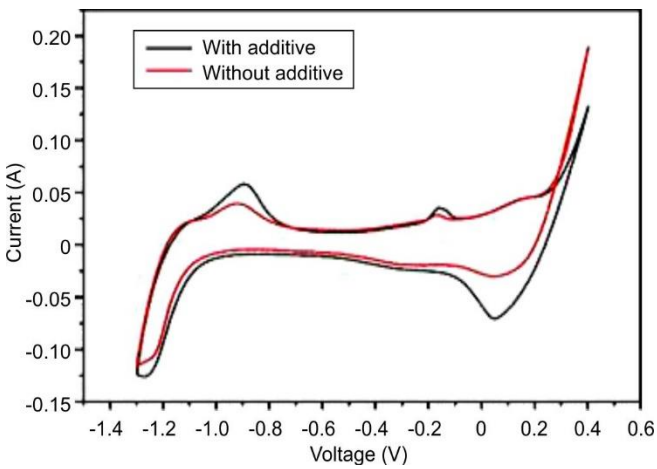

Fig. 5. Cyclic voltammograms recorded at 5 mV/s for the Ni–Cd cell in the absence and presence of oxadiazole additive

All EIS, CA, and CV results consistently indicate that the additive enhances electrochemical reversibility, reduces interfacial and diffusion resistances, suppresses parasitic reactions and improves the redox kinetics relevant to capacity. Consequently, the additive-treated Ni-Cd cell exhibits higher discharge capacity, improved rate capability, reduced self-discharge, and enhanced cycling stability compared to the additive-free system.

Charge-discharge studies: Discharge potentials were recorded at different time intervals during the charge-discharge experiments. These experiments were conducted both in the absence and presence of the organic electrolyte additive, 5-(4-(dimethylamino)phenyl)-1,3,4-oxadiazole-2(3*H*)-thione. The charge–discharge studies were performed at varying discharge rates at 303 ± 1 K.

Capacity output studies: The output capacities of electrodes and cells have also been studied without and with the organic additives (CMC), organic electrolyte additives and the results have been tabulated in Tables 2 and 3.

TABLE-2
DATA OF OUTPUT CAPACITY OF SINGLE CELL WITH AND WITHOUT ADDITIVE AT DIFFERENT RATES

Output capacities of electrodes	No. of charge discharge cycles		
	Blank	CMC	5-(4-(Dimethylamino)-phenyl)-1,3,4-oxadiazole-2(3*H*)-thione
0.1	28	29	25
0.5	26	27	25
1.0	22	23	23

TABLE-3
DATA OF OUTPUT CAPACITY OF SINGLE CELL WITH AND WITHOUT ADDITIVES AT DIFFERENT RATES

Output capacities of electrodes	No. of charge discharge cycles		
	Blank	CMC	5-(4-(Dimethylamino)-phenyl)-1,3,4-oxadiazole-2(3*H*)-thione
0.5	24	25	25
1.0	23	24	25

Discharge mechanism and fabrication of porous electrodes: Discharge profiles typically exhibit three characteristic regions. An initial rapid drop in potential is observed, associated with activation processes, followed by a relatively gradual decline governed by ohmic resistance. In the final stage, a sharp decrease in voltage occurs, primarily due to mass transport limitations. This terminal decline is inherently non-linear and may arise from phenomena such as crystallisation or depletion of electroactive species; it is particularly important as it marks the end of the usable discharge capacity of the cell.

At moderate discharge rates, the voltage profile remains nearly flat over a substantial portion of the discharge period, indicating stable electrochemical behaviour until the active material becomes depleted. However, when the discharge current exceeds the rated value, the voltage curve exhibits a steeper slope, leading to a lower cut-off voltage and a reduction in the achievable ampere-hour capacity per cycle. During discharge, the electrolyte concentration gradually decreases,

resulting in increased internal resistance. Simultaneously, limitations in mass transport become more pronounced due to restricted diffusion of active species, particularly when materials exhibit low diffusion coefficients. To mitigate electrode polarisation under such conditions, the active materials for both electrodes were prepared with a controlled porous structure, facilitating improved electrolyte access and ion transport.

Failure mechanisms of sintered cadmium electrodes and role of additives: The performance limitations of sintered cadmium electrodes in Ni-Cd systems are closely associated with the structural and kinetic constraints arising during repeated cycling. A key challenge lies in the progressive accumulation of $Cd(OH)_2$ within the porous matrix during discharge, which restricts ionic transport and reduces the availability of the electrochemically active sites [38]. This effect is further intensified by the formation of crystalline $Cd(OH)_2$ phases whose size, morphology and distribution depend strongly on the charge–discharge of electrode [39]. As a result, the electrode undergoes gradual loss of efficiency due to diffusion limitations within the growing hydroxide layer.

In addition to mass transport constraints, the intrinsic properties of the β-$Cd(OH)_2$ phase, including lattice structure, crystallite size and surface characteristics, play a decisive role in governing discharge behaviour [40]. The repeated dissolution-precipitation processes during cycling promote the formation of a dense and poorly conductive $Cd(OH)_2$ film on the cadmium surface. This layer progressively inhibits charge transfer, leading to increased polarisation and eventual onset of parasitic reactions such as oxygen evolution under sustained current conditions [41]. Interfacial degradation mechanisms play a central role in the observed decline in discharge efficiency.

The evolution of electrode microstructure with cycling further contributes to performance deterioration. Although freshly prepared electrodes exhibit relatively high surface areas, continuous cycling leads to redistribution and agglomeration of active material, resulting in a measurable reduction in effective surface area and electrochemical accessibility [42,43]. Moreover, at higher discharge currents, the formation of intermediate species (*e.g.* CdO) and their incomplete conversion to $Cd(OH)_2$ introduces additional kinetic barriers, thereby reducing the attainable capacity. The partial recovery of capacity upon subsequent low-current discharge suggests that these limitations are at least partly reversible and governed by diffusion-controlled processes [44].

Previous studies have demonstrated that the incorporation of suitable additives can mitigate several of these limitations by modifying interfacial and transport properties [45]. For instance, additives such as benzotriazole have been shown to stabilise discharge capacity across a wide range of operating conditions, particularly by reducing the rate of capacity fade at higher currents. These improvements have been attributed to enhanced cadmium dissolution kinetics and reduced diffusion resistance within the hydroxide layer. Despite reported improvements, the fundamental mechanisms through which additives modulate film formation, ion transport and structural evolution at the electrode interface remain inadequately elucidated. In this context, the present study explores the incorporation of trace metallic additives, such as cobalt and zinc, during electrode preparation as a strategy to control $Cd(OH)_2$ formation and preserve pore accessibility. By limiting the development of compact hydroxide layers and facilitating more uniform reaction pathways, these additives are expected to reduce polarisation effects and enhance overall discharge performance. This approach addresses a critical gap in existing studies by focusing not only on performance enhancement but also on the underlying physico-chemical mechanisms governing electrode behaviour in alkaline Ni-Cd systems.

Effect of electrolyte composition on cell performance: The composition of electrolyte influences the performance of alkaline cells in different ways. The effect of electrolyte concentration on the performance of the cell and the effect of additives such as lithium hydroxide and other inorganic and organic additives are debatable subjects of great importance. The effect of electrolyte composition on different types of Ni-Cd cells can be analysed before interpreting the results of the present work.

Ni-Cd pocket cells: Normally, pocket cells are filled with electrolyte containing 19-24% of KOH, corresponding to a density of 1.18-1.23 g/mL at room temperature. At densities below 1.18 g/mL; the cell capacity tends to decrease and this tendency is more pronounced at low temperature. Further, a decrease in density is accompanied by decreased conductivity and higher freezing point. At 1.23 g/mL, the electrolyte does not start to freeze until it is at -36 ºC, the corresponding value for 1.18 g/mL is -23 ºC. Since satisfactory operation at -18 ºC to -15 ºC is frequently required, a density of at least 1.17 g/mol is necessary. Therefore, in this work focusing on electrolyte composition, a KOH solution with a density of 1.17 g/mL was consistently employed in all test cells.

Ni-Cd sintered plate cells: The vented sintered plate cells are normally filled with solution of pure KOH containing 26-32% by weight of KOH. As the conductivity is maximum at 27% KOH and the lowest freezing point of -66 ºC is at 31% KOH, the normal range is between 27 to 31%. However, a capacity improvement of 6% can be obtained while using 35% KOH compared with often used 31% KOH electrolyte. For very low temperature applications higher concentrations have been considered favourable.

A higher KOH concentration has certain negative effects also (i) the cycle life of the positive electrodes may be decreased (ii) the oxygen recombination rate in sealed cells will decrease with increasing KOH concentration. These effects occur probably due to the reduced solubility of oxygen in the more concentrated electrolytes. Thus, the lowest possible concentration of KOH used should be compatible with freezing and increased internal resistance considerations. In present study, taking into consideration the above facts and the proposed utilisation of the cell for low temperatures applications, the concentration of KOH is maintained at 35%.

Effect of electrolyte additives on cell performance: A mixed electrolyte containing 35% KOH, 1% LiOH and 0.5% 5-(4-(dimethylamino)phenyl)-1,3,4-oxadiazole-2(3*H*)-thione was used.

Capacity tests and performance of cells: Tables 2 and 3 summarise the capacity output obtained from both single-electrode and full-cell configurations in the presence and absence of different electrolyte additives. The results indicate

a clear enhancement in capacity at lower discharge rates (0.1 C and 0.5 C) for all additive-containing systems compared to additive-free cells. This improvement can be attributed to the role of the additives in suppressing the nucleation and growth of $Cd(OH)_2$ within the porous electrode matrix, thereby preserving pore accessibility and promoting a more uniform distribution of active material.

A distinct variation in performance is observed during cycling. In the initial cycles, cells containing organic additive exhibit comparatively lower capacity than those incorporating CMC. However, from the 7th-8th cycle onwards, a progressive improvement in capacity is evident for the oxadiazole based additive. The capacity reaches a maximum across both low and high discharge rates by approximately the 10th cycle, and a stable output is attained around the 12th cycle, indicating improved electrode conditioning and stabilisation of electrochemical processes.

The half-cell potential measurements further support these observations. In cells containing oxadiazole derivative, the electrode potential remains below 1.30 V during discharge, whereas in additive-free systems it increases to nearly 1.40 V under similar conditions. This reduction in potential suggests that the adsorbed layer of organic additives, including both CMC and the oxadiazole derivative, decreases interfacial resistance and facilitates charge transfer. In addition, the utilisation efficiency during the first cycle exceeds 80% of the theoretical capacity in the presence of oxadiazole derivative, which is higher than that observed for CMC-treated and untreated systems. The utilisation capacity further improves with increasing cycle number, reflecting enhanced activation and more effective utilisation of the electrode material over prolonged cycling.

Charge-discharge characteristics: Fig. 6 indicates that although the initial discharge potential of cells containing oxadiazole derivative is comparatively lower than that of CMC-added and additive-free systems, the potential in the later stages of discharge is significantly improved. In this region, the oxadiazole based additive exhibits a higher and more stable discharge potential than CMC, ultimately resulting in superior overall performance relative to both CMC-containing and blank cells. These observations suggest that the role of the oxadiazole-based additive extends beyond

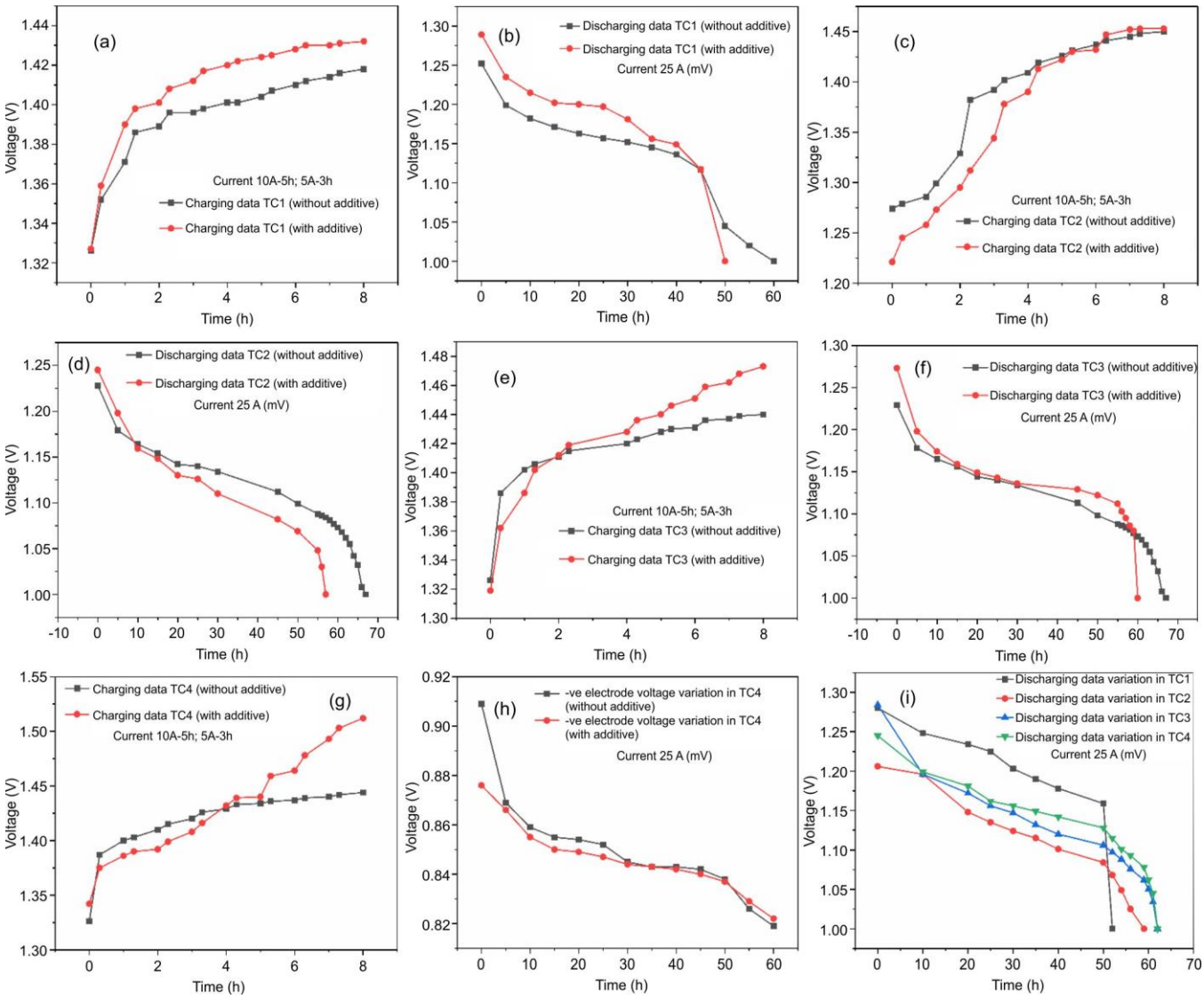

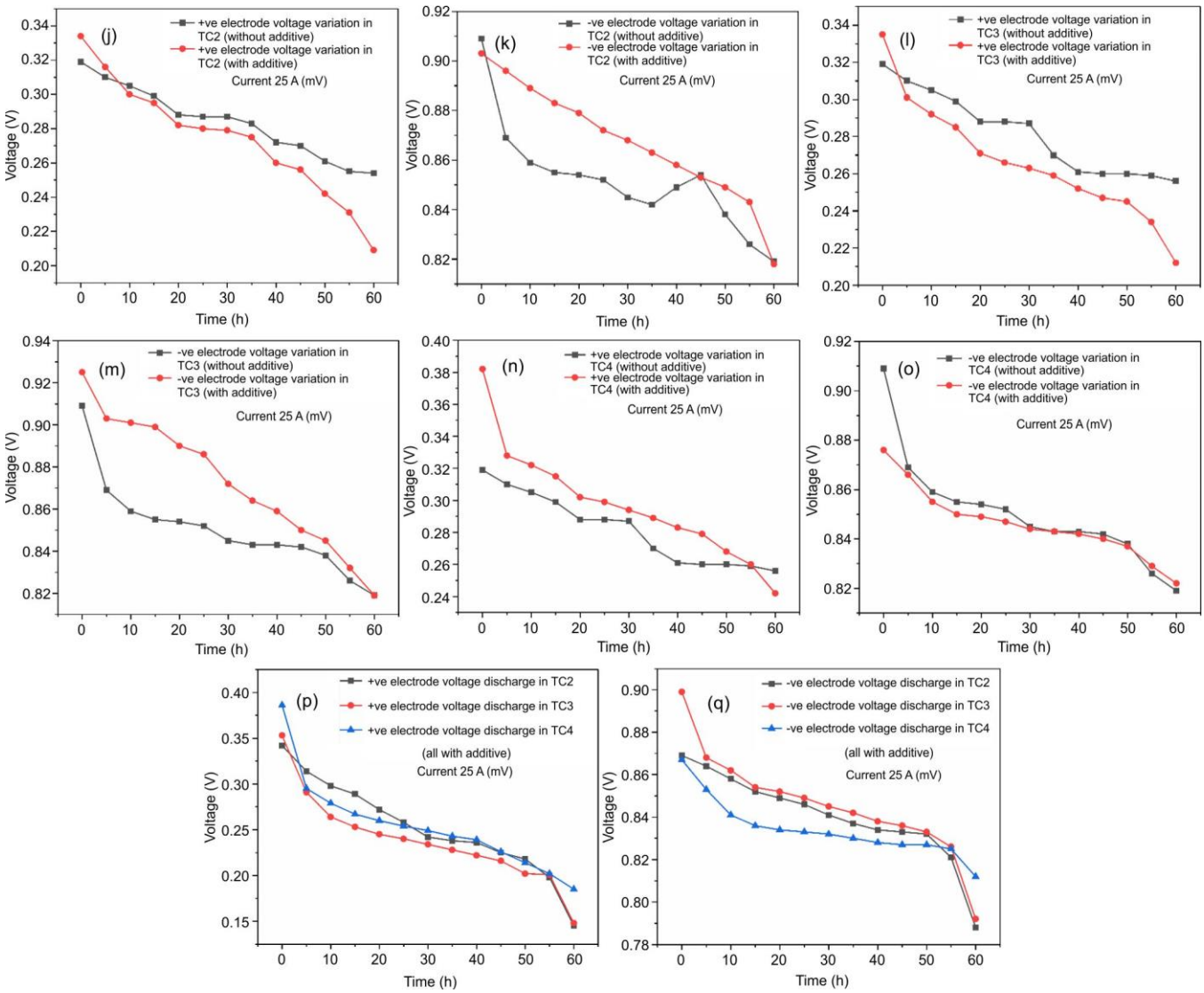

Fig. 6. Comparative electrochemical performance of Ni-Cd cells with blank, CMC and oxadiazole added electrolytes: (a) charging data in TC1, (b) discharging data in TC1, (c) charging data in TC2, (d) discharging data in TC2, (e) charging data in TC3, (f) discharging data in TC3, (g) charging data in TC4, (h) discharging data in TC4, (i) variation of discharge profiles over successive cycles, (j) positive electrode voltage variation in TC2, (k) negative electrode voltage variation in TC2, (l) positive electrode voltage variation in TC3, (m) negative electrode voltage variation in TC3, (n) positive electrode voltage variation in TC4, (o) negative electrode voltage variation in TC4, and (p) variation of positive electrode and (q) negative electrode discharge voltage in additive-containing cells

conventional surface passivation. While adsorption at the electrode surface does occur, the additive appears to form a thin, permeable interfacial layer that facilitates ion transport while simultaneously suppressing undesirable side reactions. The marked reduction in charge-transfer resistance, along with improved redox reversibility and enhanced discharge characteristics, indicates that kinetic enhancements dominate over simple surface blocking effects. Selective adsorption of the additive contributes to interfacial stabilisation, enabling improved charge-transfer processes and maintaining electrochemical activity during cycling. The proposed mechanism, illustrated in Fig. 7, highlights the multifunctional role of the additive at the electrode–electrolyte interface, including reduction of interfacial resistance, suppression of parasitic reactions, stabilisation of the interface and enhancement of redox kinetics in Ni–Cd systems.

Conclusion

The present study demonstrates that addition of 5-(4-(dimethylamino)phenyl)-1,3,4-oxadiazole-2(3*H*)-thione into a 35% KOH electrolyte markedly enhances the electrochemical performance of Ni-Cd cells. The structural confirmation of the synthesised additive by FTIR and NMR is supported by electrochemical analyses, which indicate a significant modification of the electrode–electrolyte interfacial behaviour. EIS reveals a distinct reduction in charge-transfer resistance and interfacial polarisation, reflecting improved ionic mobility and more favourable electrode kinetics in the presence of additive. The cyclic voltammetry and chronoamperometric studies further confirm enhanced reversibility of redox processes, suppression of parasitic reactions and increased utilisation of electroactive species. Charge–discharge cycling studies show

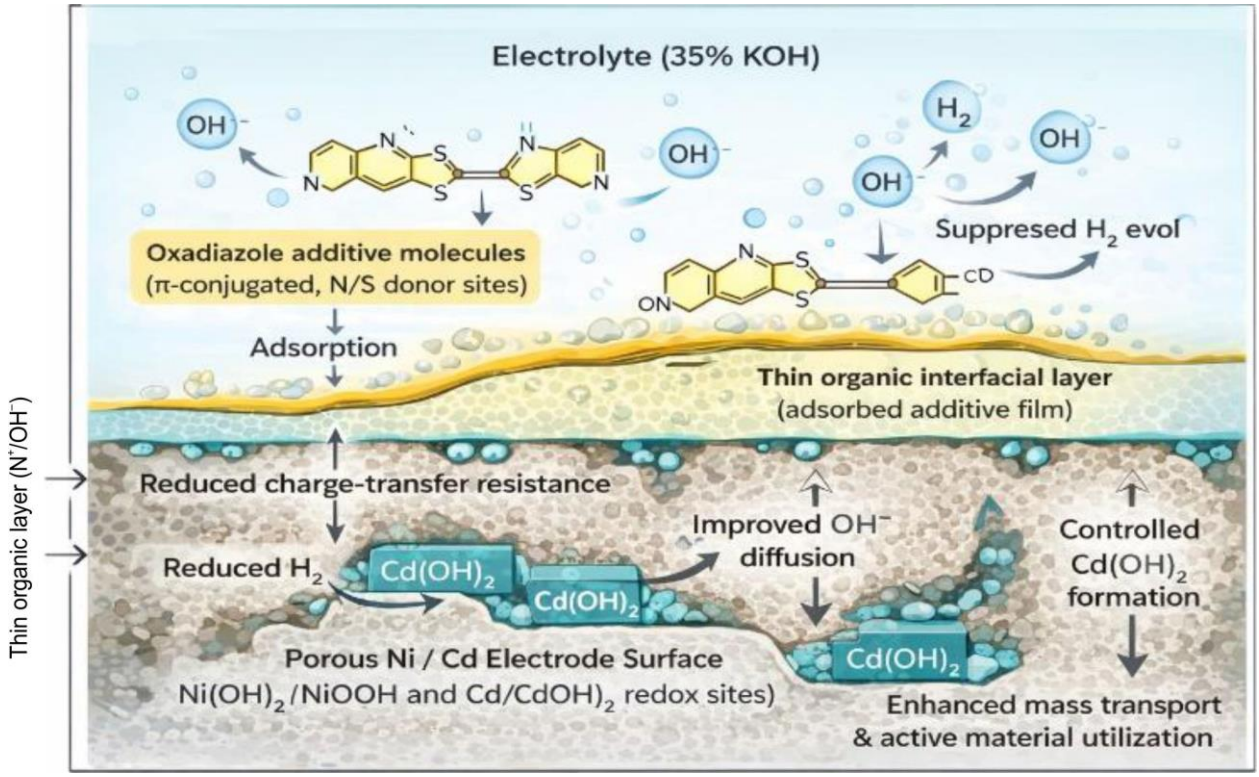

Fig. 7. Schematic illustration explaining the proposed mechanism of oxadiazole additive action at the electrode–electrolyte interface

that cells containing the oxadiazole-based additive consistently exhibit higher discharge potentials in the later stages of discharge, along with improved capacity retention compared to both additive-free and CMC-modified systems. The additive appears to mitigate the formation and accumulation of $Cd(OH)_2$ within the porous cadmium electrode, thereby reducing mass transport limitations associated with pore blockage and structural degradation. Enhanced diffusion characteristics and stabilisation of the electrode surface contribute to improved coulombic efficiency and more effective utilisation of active material during prolonged cycling. The capacity measurements further indicate that the additive promotes superior performance at low and intermediate discharge rates, particularly beyond the seventh cycle, where stable and enhanced capacity trends are observed. The reduction in half-cell potentials and improved discharge profiles highlight the role of the additive in lowering interfacial resistance and facilitating charge-transfer processes. Based on the obtained results, 5-(4-(dimethylamino)phenyl)-1,3,4-oxadiazole-2(3*H*)-thione is established as an effective electrolyte modifier capable of enhancing electrochemical reversibility, rate capability and long term stability of the Ni-Cd systems.

CONFLICT OF INTEREST

The authors declare that there is no conflict of interests regarding the publication of this article.

DECLARATION OF AI-ASSISTED TECHNOLOGIES

During the preparation of this manuscript, the authors used an AI-assisted tool(s) to improve the language. The authors reviewed and edited the content and take full responsibility for the published work.

REFERENCES

1. B. Bhawna, P. Phogat, S. Shreya, N.L. Singh and S. Singh, *React. Chem. Eng.*, **10**, 2764 (2025); https://doi.org/10.1039/D5RE00156K
2. K.V.N. Kotkunde, A. Ashwin, A. Gosavi and M. Gaur, *IOP Conf. Ser.: Mater. Sci. Eng.*, **1123**, 012022 (2021); https://doi.org/10.1088/1757-899X/1123/1/012022
3. K. Pourabdollah, *Chem. Eng. Sci.*, **160**, 304 (2017); https://doi.org/10.1016/j.ces.2016.11.038
4. S.S. Zhang, *J. Power Sources*, **162**, 1379 (2006); https://doi.org/10.1016/j.jpowsour.2006.07.074
5. K. Xu, *Chem. Rev.*, **114**, 11503 (2014); https://doi.org/10.1021/cr500003w
6. E. Sharma, A. Singh, K. Singh, S.S. Ganti, G.D. Gupta and S.K. Verma, *Electrocatalysis*, **16**, 773 (2025); https://doi.org/10.1007/s12678-025-00962-6
7. P. Zhang, B. Xia, Q. Zhang, B. Yang, M. Li, G. Zhang and W. Tian, *Synth. Met.*, **156**, 705 (2006); https://doi.org/10.1016/j.synthmet.2006.03.011
8. F. Li, Z. Wei, A. Manthiram, Y. Feng, J. Ma and L. Mai, *J. Mater. Chem. A Mater. Energy Sustain.*, **7**, 9406 (2019); https://doi.org/10.1039/C8TA11999F
9. A. Vishwakarma, A. Shukla, S.P. Sonkar, S. Singh, D. Mitra, R. Chandra, S. Yadav, A. Acharya and M.K. Bharty, *J. Mol. Struct.*, **1334**, 141781 (2025); https://doi.org/10.1016/j.molstruc.2025.141781
10. X. Jiang, S. Deng, J. Liu, N. Qi and Z. Chen, *ACS Appl. Energy Mater.*, **4**, 4610 (2021); https://doi.org/10.1021/acsaem.1c00230
11. P. Stelmachowski, J. Duch, D. Sebastián, M.J. Lázaro and A. Kotarba, *Materials*, **14**, 4984 (2021); https://doi.org/10.3390/ma14174984

12. K. Breimaier, Master's Thesis, Electrochemical and Computational Studies of Heterocyclic Corrosion Inhibitors, University of Akron, OH, USA (2023).
13. A. Thoume, D.B. Left, A. Elmakssoudi, R. Achagar, M. Dakir, M. Azzi, and M. Zertoubi, *Langmuir*, **38**, 7472 (2022); https://doi.org/10.1021/acs.langmuir.2c00441
14. G.K. Inwati, V.K. Yadav, I.H. Ali, S.B. Vuggili, S.D. Kakodiya, M.K. Solanki, K.K. Yadav, Y. Ahn, S. Yadav, S. Islam and B.-H. Jeon, *Appl. Sci.*, **12**, 3753 (2022); https://doi.org/10.3390/app12083753
15. S.R. Pattan, P.A. Rabara, J.S. Pattan, A.A. Bukitagar, V.S. Wakale, and D.S. Musmade, *Indian J. Chem.*, **48**, 1453 (2009).
16. H.F. Shurvell, Spectra-Structure Correlations in the Mid- and Far-Infrared, In: Handbook of Vibrational Spectroscopy, vol. 3, pp. 1783-1816 (2006).
17. L. Morsch, S. Farmer, K. Cunningham, Z. Sharrett and D. Kennepohl, Infrared Spectra of Some Common Functional Groups, Organic Chemistry, LibreTexts, pp. 1-10 (2022).
18. S. Bala, S. Kamboj, A. Kajal, V. Saini and D.N. Prasad, *BioMed Res. Int.*, **2014**, 172791 (2014); https://doi.org/10.1155/2014/172791
19. N.K. Singh and S. Ganguly, *ChemistrySelect*, **10**, e202500769 (2025); https://doi.org/10.1002/slct.202500769
20. A.C. Lazanas and M.I. Prodromidis, *ACS Meas. Sci. Au*, **3**, 162 (2023); https://doi.org/10.1021/acsmeasuresciau.2c00070
21. A. Lasia, Electrochemical Impedance Spectroscopy and its Applications, In: Modern Aspects of Electrochemistry, Boston, MA, USA: Springer US, pp. 143-248 (2002);
22. W. Choi, H.C. Shin, J.M. Kim, J.Y. Choi and W.S. Yoon, *J. Electrochem. Sci. Technol.*, **11**, 1 (2020); https://doi.org/10.33961/jecst.2019.00528
23. N. Al-Zubaidi R-Smith, M. Kasper, P. Kumar, D. Nilsson, B. Mårlid and F. Kienberger, *Batteries*, **8**, 50 (2022); https://doi.org/10.3390/batteries8060050.
24. R.A. Márquez, K. Kawashima, Y.J. Son, G. Castelino, N. Miller, L.A. Smith, C.E. Chukwuneke and C.B. Mullins, *ACS Energy Lett.*, **8**, 1141 (2023); https://doi.org/10.1021/acsenergylett.2c02847
25. S. Begum, V. Muralidharan and C. Ahmedbasha, *Int. J. Hydrogen Energy*, **34**, 1548 (2009); https://doi.org/10.1016/j.ijhydene.2008.11.074
26. H.J. Kim, C. Senthil, Y.C. Kim and H.Y. Jung, *J. Power Sources*, **656**, 238043 (2025); https://doi.org/10.1016/j.jpowsour.2025.238043
27. S. Hosseini, S.J. Han, A. Arponwichanop, T. Yonezawa and S. Kheawhom, *Sci. Rep.*, **8**, 11273 (2018); https://doi.org/10.1038/s41598-018-29630-0
28. A.J. Bard, L.R. Faulkner and H.S. White, Electrochemical Methods: Fundamentals and Applications. Hoboken, NJ, USA: John Wiley & Sons (2022).
29. A. Lasia, Definition of Impedance and Impedance of Electrical Circuits, In: Electrochemical Impedance Spectroscopy and Its Applications, New York, NY, USA: Springer New York, pp. 7-66 (2013).
30. W. Dai, L. Lin, Y. Li, F. Li and L. Chen, *Int. J. Hydrogen Energy*, **44**, 28746 (2019); https://doi.org/10.1016/j.ijhydene.2019.09.095
31. D. Pavlov, Lead-Acid Batteries: Science and Technology, Elsevier: Amsterdam, The Netherlands (2011).
32. L. Bing, Y. Huatang, Z. Yunshi, Z. Zuoxiang and S. Deying, *J. Power Sources*, **79**, 277 (1999); https://doi.org/10.1016/S0378-7753(99)00053-1
33. D.S. Hall, C. Bock and B.R. MacDougall, *J. Electrochem. Soc.*, **160**, F235 (2013); https://doi.org/10.1149/2.026303jes
34. H. Bode, K. Dehmelt and J.J.E.A. Witte, *Electrochim. Acta*, **11**, 1079 (1966); https://doi.org/10.1016/0013-4686(66)80045-2
35. B. Ash, V.S. Nalajala, A.K. Popuri, T. Subbaiah and M. Minakshi, *Nanomaterials*, **10**, 1878 (2020); https://doi.org/10.3390/nano10091878
36. S. Yan, K.H. Young and K.S. Ng, *Batteries*, **1**, 54 (2015); https://doi.org/10.3390/batteries1010054
37. X. Yi, V. Celorrio, H. Zhang, N. Robertson and C. Kirk, *J. Mater. Chem. A Mater. Energy Sustain.*, **11**, 22275 (2023); https://doi.org/10.1039/D3TA04731H
38. R. Barnard, G.S. Edwards, J.A. Lee and F.L. Tye, *J. Appl. Electrochem.*, **6**, 431 (1976); https://doi.org/10.1007/BF00616543
39. F.P. Kober, *J. Electrochem. Soc.*, **112**, 1064 (1965); https://doi.org/10.1149/1.2423361
40. M. Wehrens-Dijksma and P.H.L. Notten, *Electrochim. Acta*, **51**, 3609 (2006); https://doi.org/10.1016/j.electacta.2005.10.022
41. S. Cho, K.H. Shin and J. Jang, *ACS Appl. Mater. Interfaces*, **5**, 9186 (2013); https://doi.org/10.1021/am402702y
42. D. Zhang, J. Lu, C. Pei and S. Ni, *Adv. Energy Mater.*, **12**, 2103689 (2022); https://doi.org/10.1002/aenm.202103689
43. A.K. Singh, M. Ravi, M.S. Bisht, R.K. Barik, S.K. Shukla, R. Prajesh, T.P. Singh, S.K. Saini and R.S. Raju, *IEEE Trans. Electron Dev.*, **62**, 3837 (2015); https://doi.org/10.1109/TED.2015.2478970
44. X. Wang, K. Cheng, S. Dou, Q. Chen, J. Wang, Z. Song, J. Zhang and H. Song, *Appl. Surf. Sci.*, **476**, 136 (2019); https://doi.org/10.1016/j.apsusc.2019.01.044
45. S. Tamil Selvan, R. Sabapathi and N. Venkatakrishnan, *J. Appl. Electrochem.*, **21**, 646 (1991); https://doi.org/10.1007/BF01024855